International Journal of General Medicine

Dovepress
Taylor & Francis Group

Open Access Full Text Article

ORIGINAL RESEARCH

Identification and Validation of Aging-Related Genes in IgA Nephropathy in the Asian Population

Jinlian Shu, He Li, Hairong Li

Department of Nephrology, The Second People's Hospital of Hefei, Hefei Hospital Affiliated to Anhui Medical University, Hefei, Anhui, People's Republic of China

Correspondence: Jinlian Shu, Email 1210497702@qq.com

Background: IgA nephropathy (IgAN) is the most common primary glomerulonephritis worldwide. Aging is a major risk factor for progression of IgAN to end-stage renal disease. The purpose of this study was to identify and verify aging-related genes associated with IgAN through bioinformatics analysis.

Methods: Microarray datasets of GSE93798 and GSE37460 were downloaded from the Gene Expression Omnibus (GEO) database. The aging-related DEGs (AR-DEGs) associated with IgAN were analyzed using R programming software, and then Gene Ontology (GO) analysis and Kyoto Encyclopedia of Genes and Genomes (KEGG) analysis were performed. The PPI network of AR-DEGs was then constructed, and hub genes were ranked using five methods of the cytoHubba plugin in Cytoscape software. CIBERSORT algorithm was used to evaluate immune infiltration and its relationship with hub genes. Next, Nephroseq V5 online platform was used to verify and analyze the mRNA expression patterns of hub genes in IgAN patients and normal controls.

Results: A total of 372 differentially expressed genes (DEGs) were identified, of which 158 were upregulated and 214 were downregulated. GO and KEGG enrichment analyses mainly focused on regulation of macrophage-derived foam cell differentiation and PI3K-Akt signaling pathway. Based on the results of PPI network analysis, eight hub genes were identified, including AGT, ALB, CD36, EGF, KDR, LPL, MYC, and PPARGC1A. Immune infiltration analysis indicated that CD36 was closely related to immune cell infiltration. Furthermore, the expression levels of these hub genes were validated using the Nephroseq V5 online platform. Further clinical samples confirmed that CD36 was highly expressed in renal tissues of IgAN patients.

Conclusion: These findings provide new insights into potential aging-related genes associated with IgAN, which may contribute to better understanding the pathogenesis of IgAN. CD36 may have diagnostic value for aging-related IgAN.

Keywords: IgA nephropathy, aging, bioinformatics analysis, hub genes, differentially expressed genes

Introduction

IgA nephropathy (IgAN) is the most common primary glomerular disease worldwide. A biopsy-based study across multiple countries has shown that the overall population incidence of IgAN was at least 2.5 per 100,000.[1] Due to the possible unrecorded subclinical cases, the true prevalence and incidence of IgAN may be higher than reported. In addition, the incidence of IgAN varies globally. The prevalence of IgAN was significantly higher in the Asian population, accounting for 40–50% of primary glomerulonephritis in China.[2] IgAN patients are mostly young adults. However, with the increasing aging population, IgAN in the elderly has gradually become a major concern. An earlier study estimated that IgAN accounted for only 2.3% of all patients over the age of 50,[3] but recent studies have reported that the proportion of elderly IgAN patients has increased to 18.3%.[4] These data suggest that the incidence of IgAN is increasing in the elderly. Furthermore, studies show that 20–40% of IgAN patients progress to end-stage renal disease within 20 years of diagnosis.[5]

Aging, a process we cannot avoid, is determined by a complex set of biological processes. Aging is the accumulation of aging cells with poor functions in the body, which leads to the reduction or loss of physiological functions, and ultimately leads to further exacerbation of functional decompensation. The main characteristics of aging are telomere attrition and genetic and epigenetic alterations.[6,7] Many studies have shown that aging is a negative factor affecting the

Received: 18 April 2025
Accepted: 29 June 2025
Published: 12 July 2025

Graphical Abstract

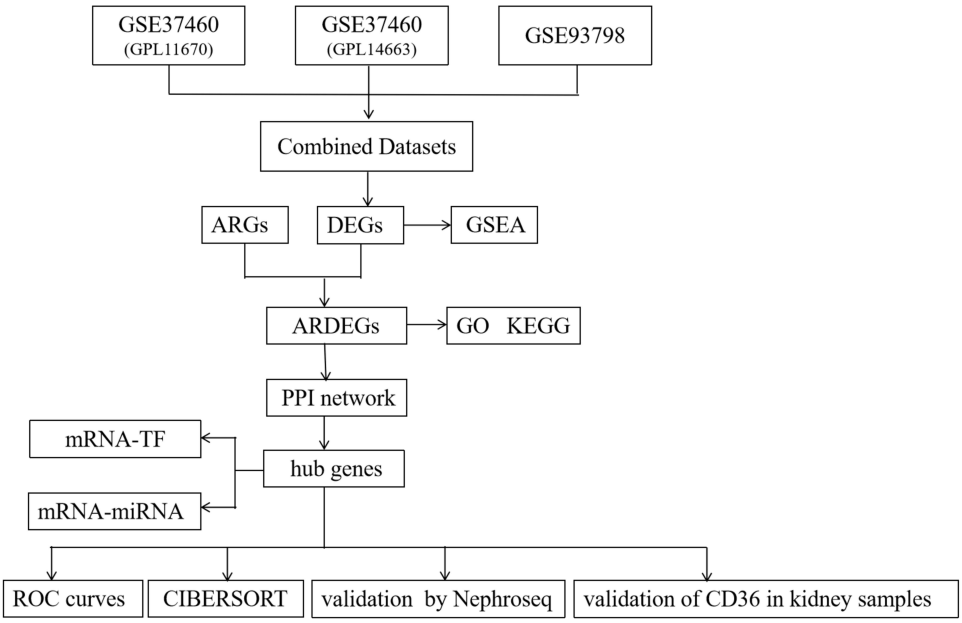

prognosis of IgAN.[8,9] A meta-analysis revealed that the incidence of end-stage renal disease in elderly IgAN patients over 50 years is 1.95 times higher than that in non-elderly IgAN patients.[10] A retrospective study comparing clinical and histopathological features between elderly and middle-aged, younger-aged IgAN patients found that elderly patients had more comorbidities, higher blood pressure, lower estimated glomerular filtration rate (eGFR) and greater proteinuria at biopsy.[11] Histological analysis of older patients exhibits more chronic changes including interstitial fibrosis/tubule atrophy and arteriosclerosis. These results were consistent with other literature reports.[12–14] Research by Moreno et al[15] demonstrated increasing incidence of IgAN among patients over 65 years old. The distinct clinical profile was characterized by hematuria-associated acute kidney injury, poor prognosis, and histological manifestations such as interstitial fibrosis. Above studies have showed that aging may be a key factor affecting the prognosis of IgAN patients, which may aggravate renal injury by promoting arteriosclerosis and interstitial fibrosis. These findings underscore the urgent need to investigate aging-related molecular pathways in IgAN pathogenesis. However, whether aging-related genes play a critical role in the development of IgAN has remained unclear. Therefore, identifying the novel aging-related genes may provide new therapeutic targets and enhance our understanding of pathogenesis in IgAN.

In addition, with regard to the pathogenesis of IgAN, the "four-hit" hypothesis is the most widely accepted and accumulating evidence supported the involvement of immune system in IgAN. T cells, B cells, monocytes and macrophages, and complement activation play crucial roles in the pathogenesis and progression of IgAN.[16] In addition, the results of single-cell RNA sequencing of peripheral blood mononuclear cells (PBMCs) showed that Th cells and B cells were more activated in IgAN patients, and the results of tissue biopsy staining demonstrated that the degree of renal CD4+T and B cell infiltration was positively correlated with the degree of renal damage.[17] Moreover, previous studies have reported that immune senescence and chronic inflammation were the main biological changes in the aging process.[18] However, whether aging-associated immune response is related to aging-related IgAN remains unclear. In consequence, in order to further explore the potential molecular mechanisms and signaling pathways between IgAN and aging, we performed bioinformatics methods to comprehensively analyze aging-related genes and their association with immune infiltration in IgAN, which will provide potential therapeutic targets and biomarkers for the treatment of IgAN.

The rapid development and widespread application of high-throughput sequencing technology and numerous public databases can effectively screen disease-related biomarkers, providing important technical support for the

prediction, diagnosis and treatment of human diseases. In this paper, we searched the gene expression profile of IgAN in the published Gene Expression Omnibus (GEO, https://www.ncbi.nlm.nih.gov/geo/) database, and then used GSE37460, GSE93798 as the object of this study. Aging-related genes were collected by integrating GeneCards database (https://www.genecards.org/)[19] and MSigDB database (https://www.gsea-msigdb.org/gsea/msigdb).[20] In this study, we used a variety of biological information analysis methods to screen aging-related IgAN genes, and verified them with Nephroseq V5 database and clinical specimens.

Materials and Methods

Microarray Data Collection

We downloaded the IgAN dataset GSE37460,[21] GSE93798[22] from the GEO database using the R package GEOquery. The samples of datasets GSE37460 and GSE93798 were all taken from human renal biopsy specimens. GSE37460 datasets were based on GPL11670 (Affymetrix Human Genome U133 Plus 2.0 Array [Hs133P_Hs_ENTREZG.cdf]) platform and GPL14663 (Affymetrix GeneChip Human Genome HG-U133A Custom CDF [Affy_HGU133A_CDF_ENTREZG_10]) platform. Among them, the GPL11670 platform data in dataset GSE37460 contained 18 healthy control samples; The GPL14663 platform data in dataset GSE37460 included 27 IgAN samples and 9 healthy control samples. Twenty IgAN samples and 22 control samples were contained in the GSE93798 dataset which was based on GPL22945 ([HG-U133_Plus_2] Affymetrix Human Genome U133 Plus 2.0 Array [CDF: Brainarray HGU133Plus2_Hs_ENTREZG_v19]) platform. The specific information was shown in S1 Table.

The GeneCards database and the MSigDB database were used to collect aging-related genes (ARGs). The GeneCards database is a searchable and comprehensive database containing almost all known human genes. We searched GeneCards database for the aging-related genes by searching "aging" as keywords, obtaining 259 ARGs and retaining only the genes with "Protein Coding" and "Relevance Score > 12". Similarly, we downloaded 110 aging-related genes from the MSigDB database by searching the keyword "aging". Subsequently, a total of 355 ARGs were finally obtained after merging and elimination of duplicates.

The datasets GSE37460 and GSE93798 were processed through the "SVA" R package to remove the batch effect and then obtained the combined GEO datasets. The combined datasets included 47 IgAN samples and 49 control samples. Finally, the combined GEO datasets were standardized and normalized with probe annotation by using "limma" package of R software. To test for batch effects, principal component analysis (PCA) of the expression matrix was performed before and after removal of batch effects. PCA is a method of dimensionality reduction of data by converting high-dimensional data to low-dimensional data and displaying these features in a two-dimensional or three-dimensional graphs.

Identification of Aging-Related Differentially Expressed Genes in IgAN

The differentially expressed genes (DEGs) between IgAN and control group in combined GEO datasets were selected using the limma R package. The cut-off criteria was set as adjusted P-value < 0.05 and |logFC| > 0.5 in the combined datasets. P values were adjusted using the Benjamini-Hochberg (BH) method. The volcano plots for the DEGs expression were plotted using R package ggplot2. Subsequently, we used R package to visually draw the Venn diagram of ARGs and DEGs, thus identifying the differentially expressed aging-related genes (AR-DEGs) associated IgAN. Heat map of AR-DEGs was shown with R package heatmap, and chromosome localization map was drawn by R package RCircos.

Gene Set Enrichment Analysis (GSEA)

Gene Set Enrichment Analysis (GSEA) was a computational method which was used to evaluate the strength of gene-phenotype correlation within a given gene set.[23] In this study, the genes in the combined GEO datasets were first sequenced according to logFC values, and then the R-package clusterProfiler was applied to implement GSEA. The parameters used in the GSEA were as follows: the seed was 2022, the number of computations was 1000, and the minimum number of genes contained in each gene set was 10 and the maximum number of genes was 500. GSEA was performed using the c2 gene sets. Cp. all. V2022.1. Hs. symbols gene sets which were obtained from the MSigDB

database. Adj.p < 0.05 and false discovery rate (FDR) q value < 0.05 were regarded as statistically significant. The p value was corrected using BH method.

GO and KEGG Enrichment Analysis

To further evaluate the biological functions and signaling pathways of AR-DEGs, we carried out Gene Ontology (GO) and The Kyoto Encyclopedia of Genes and Genomes (KEGG) analyses by clusterprofiler R package, with adj.p < 0.05 and FDR q value < 0.05 as the threshold. GO enrichment analysis included three aspects: molecular function (MF), biological process (BP) and cellular component (CC). The p value was corrected using BH method.

Protein-Protein Interaction (PPI) Network Construction and Identification of Hub Genes

In order to further assess the functional interactions among AR-DEGs, a PPI network was constructed using the Search Tool for the Retrieval of Interacting Genes (STRING) (http://string-db.org/).[24] The minimum correlation coefficient greater than 0.700 was considered to be significant. The PPI network was then visualized using Cytoscape, and hub genes were identified by cytoHubba plugin. Among them, the following five algorithms were used in Cytohubba plugin, namely maximal clique centrality (MCC), closeness, maximum neighborhood component (MNC), degree, edge percolated component (EPC). In the PPI network, the scores of AR-DEGs were computed, and then the top 10 genes were selected. The intersection of genes obtained by these five algorithms were identified as the hub genes and visually displayed by generating Venn diagrams.

Construction of Regulatory Network

Transcription factors (TF) control gene expression through interaction with hub genes during the post-transcriptional stage. To further explore the relationship between TF and the hub genes, we applied ChIPBase database (http://rna.sysu.edu.cn/chipbase/) to predict TF targeted by hub genes.[25] In addition, the miRNA-TF interaction pairs were screened using the sum of number of samples found (upstream) and number of samples found (downstream) greater than 4 as thresholds. Then, the mRNA-TF regulatory network was visualized by Cytoscape software.

MiRNA plays an important regulatory role in the process of biological processes. A single miRNA can regulate multiple target genes, while multiple miRNAs can target a single gene. To better understand the correlation between hub genes and miRNA, we used the ENCORI database to analysis mRNA-miRNA interaction.[26] PancancerNum > 8 was regarded as the screening criteria for mRNA-miRNA. Then, the mRNA-miRNA co-regulation network was visualized through Cytoscape.

Differential Expression Verification and ROC Curve Analysis of Hub Genes

To further verify hub genes, we used R language to analyze the differences in hub genes expression between IgAN group and control group. Differences in the expression of hub genes between IgAN group and control group were compared using Mann–Whitney test (Wilcoxon rank sum test) in combined datasets. The area under the curve (AUC) of the ROC curve was used to validate the diagnostic efficiency of IgAN using the "pROC" R package based on hub genes.

Immune Infiltration Analysis

CIBERSORT is based on the principle of linear support vector regression to deconvolute the transcriptome expression matrix to estimate the composition and abundance of immune cells in the mixed cells.[27] The results of immune cell infiltration matrix in the combined datasets were finally obtained through CIBERSORT combined with LM22 signature matrix. Subsequently, immune cells with significant differences between IgAN group and control group were screened for subsequent analysis. The correlation between hub genes and immune cells was computed using Spearman correlation, and bubble plots were drawn in R using the ggplot2 package.

Nephroseq V5 Validation

In order to verify the expression level of hub genes in IgAN, we used Nephroseq V5 online platform (http://v5.nephroseq.org) to analyze hub genes.[28] Group data were represented as mean ± standard deviation. Student's *t* test was used to compare the differences between two groups. Statistical significance was shown as $^{*}p < 0.05$, $^{**}p < 0.01$, $^{***}p < 0.001$.

Immunohistochemistry Staining

The clinical renal tissue sample validation study was conducted in accordance with the Helsinki Declaration with the consent of the Ethics Committee of the Second People's Hospital of Hefei. The kidney biopsy specimens were collected by percutaneous renal puncture biopsy technique in the department of nephrology from January 2021 to May 2024. The kidney tissue samples were prepared according to standardized methods and analyzed by light microscopy, electron microscopy and immunofluorescence microscopy, respectively, in the department of pathology. A total of 22 patients with IgAN were included as the case group. The control group consisted of 10 samples of histologically non-neoplastic renal parenchyma obtained from age-matched individuals undergoing renal tumor resection surgery. Tissues were sampled at least 5 cm from the tumor site during resection surgery, and histologic evaluation confirmed the absence of chronic kidney disease, glomerular injury, or interstitial fibrosis. The inclusion criteria for IgAN were (1) age ≥ 18 years; (2) No corticosteroids and immunosuppressive therapy were used within one month prior to enrollment; (3) CKD stages 1–4, eGFR was calculated using CKD-EPI formula. Exclusion criteria: (1) diagnosis of secondary IgAN, including liver disease, anaphylactoid purpura, ulcerative colitis, systemic lupus erythematosus, tumors, etc.; (2) Combined with infection, malignant hypertension, cardiac insufficiency, etc.; (3) The follow-up data were incomplete. The biochemical data for patients were summarized in Table 1.

Paraffin-embedded kidney sections were dewaxed in xylene and hydrated in ethanol. Antigen retrieval was performed on tissue samples with EDTA buffer (pH 9.0) in a pressure cooker for 2 min. Subsequently, the slices were then incubated at room temperature in 3% hydrogen peroxide for 10 minutes to block endogenous peroxidase activity, rinsed three times with distilled water followed by PBS-T. After washing, the sections were capped and incubated with the primary anti-CD36 antibody (Bioss, 1:300) for 60 min at 37°C. Following the antibody incubation, the slices were removed from the incubator and rinsed with PBS-T for 3 times. Then, the extra liquid was blotted off, and the slices were incubated with HRP-conjugated secondary antibodies at 37°C for 30 min. Subsequently, the slices were removed again and rinsed 3 times with PBS-T. Removal of excess liquid, the slices were incubated in the DAB solution until developed brown color.

Table 1 Clinical Characteristics

Parameters	Control (n = 10)	IgAN (n = 22)	p
Male n (%)	80%	72.7%	0.512
Age (year)	41.5±6.43	41.68±12.82	0.967
BUN (mmol/L)	5.08±0.82	6.38±2.44	0.033
Cr (μmol/L)	72.43±12.71	95.88±34.79	0.009
UA (μmol/L)	333.14±68.66	388.52±95.13	0.109
TC (mmol/L)	4.24(3.79,4.86)	4.44(3.73,5.39)	0.509
TG (mmol/L)	1.32±1.00	1.99±1.09	0.106
Alb (g/L)	40.94±3.29	34.85±7.56	0.021
BMI (kg/m^2)	22.99±1.13	23.29±1.75	0.623
SBP (mmHg)	118.80±9.92	131.73±13.91	0.013
DBP (mmHg)	66.20±6.27	78.73±11.12	0.002
MAP (mmHg)	83.73±7.13	96.39±10.22	0.001
Hb (g/L)	135.4±7.72	130.41±7.21	0.086
eGFR ($mL/min.1.73m^2$)	107.39±9.51	93.40(60.77,118.52)	0.021
24h-pro (g/24h)		1.035(0.530,2.233)	

Abbreviations: BUN, blood urea nitrogen; Cr, creatinine; UA, uric acid; TC, total cholesterol; TG, triglycerides; Alb, albumin; SBP, systolic blood pressure; DBP, diastolic blood pressure; MAP, mean arterial pressure; Hb, hemoglobin; eGFR, estimated glomerular filtration rate.

The sections were then rinsed with distilled water and counterstained with hematoxylin, rendered transparent by xylene. Finally, the results were observed under an optical microscope after the sections were sealed with neutral gum. Five random visual fields were selected for per section, and then the positively stained areas were calculated using Image J software.

Statistical Analysis

Statistical analysis was performed using R (version 4.3.1) and SPSS (version 20.0), while protein expression levels in immunohistochemical images were quantified using ImageJ (version 2.3.0). Measurement data that meet the criteria of normality and homogeneity of variance were expressed as mean±standard deviation (x±s); otherwise, they were presented as median (M) and interquartile range (p25, p75). When the assumptions of normality and homogeneity of variance were satisfied, the *t*-test was used to compare the means of two groups. For non-normally distributed variables, the Mann–Whitney *U*-test was applied. Categorical data were expressed as percentages, and comparisons between percentages were performed using the chi-square (χ^2) test. P value < 0.05 was considered statistically significant.

Results

Identification of DEGs and AR-DEGs in IgAN

First, to obtain DEGs related IgAN, we used R-packet sva to eliminated batch effects from the gene expression matrix after merging the GSE37460 and GSE93798 datasets. The box diagram (Figure 1A and B) clearly presented that the difference in the expression values of the datasets before and after batch impact removal. In addition, the principal component analysis also showed that the distribution of datasets before and after removing batch effects (Figure 1C and D). The above results showed that the sample distributions among IgAN datasets were consistent after removing the batch impact. After the microarray results were normalized, totally 372 DEGs involved in IgAN were identified by limma package (adj.p < 0.05, | logFC| > 0.5), of which 158 genes were up-regulated and 214 genes were down-regulated. The volcano plot was represented in Figure 2A. Subsequently, 20 AR-DEGs were obtained by intersection of DEGs involved in IgAN with 355 aging-related genes, namely ABCB1, AGT, AGTR1, ALB, ARG2, C3, CD36, CDKN1A, COL1A1, CX3CR1, EG, GHR, HBB, HLA-DQB1, KDR, LPL, MYC, PPARGC1A, SERPINE1, and TWIST1. A Venn diagram was shown in Figure 2B. Heat map of AR-DEGs in the IgAN groups and control groups was displayed using R package heatmap (Figure 2C). R-package RCircos was used to draw a chromosome localization map of AR-DEGs. The chromosome localization diagram showed that more genes were located on the 4 and 7 chromosome (Figure 2D). ALB, EGF, KDR, and PPARGC1A were located on chromosome 4, whereas ABCB1, CD36, SERPINE1, and TWIST1 were located on chromosome 7.

Gene Set Enrichment Analysis (GSEA)

We performed GSEA to explore the potential functions and the key pathways in IgAN (Figure 3A). The results suggested that most of the enriched gene sets were significantly enriched in reactome assembly of collagen fibrils and other multimeric structures (Figure 3B), reactome signaling by NOTCH4 (Figure 3C), reactome negative regulation of NOTCH4 signaling (Figure 3D), reactome costimulation by the CD28 family (Figure 3E), reactome met promotes cell motility (Figure 3F), wikipathways inflammatory response pathway (Figure 3G), reactome hedgehog ligand biogenesis (Figure 3H) and other biologically relevant functions and signaling pathways. Specific details of the results were summarized in S2 Table.

Go and KEGG Enrichment Analysis of AR-DEGs

In order to further assess the potential biological signature of these AR-DEGs, we then performed GO and KEGG enrichment analysis using R software. As shown in the S3 Table, the GO analysis showed that AR-DEGs were significantly enriched in biological processes (BP), including positive regulation of macrophage derived foam cell differentiation, nitric oxide biosynthetic process, nitric oxide metabolic process, reactive nitrogen species metabolic process, regulation of macrophage derived foam cell differentiation, macrophage derived foam cell differentiation. GO molecular function (MF) was notably concentrated in growth factor binding, G protein-coupled receptor binding, cytokine binding, lipoprotein particle binding,

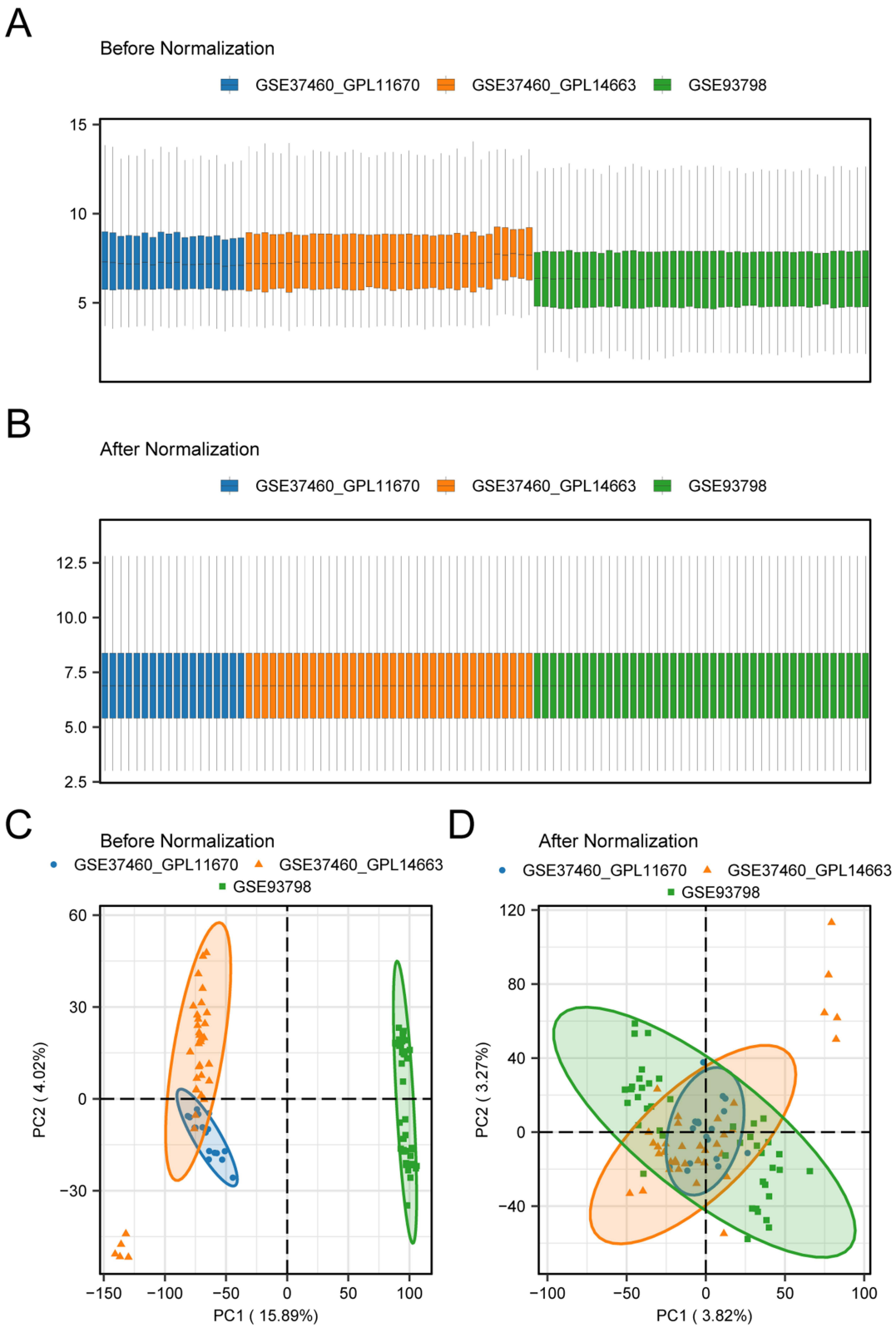

Figure 1 GEO datasets de-batching. (**A**) Box plot of the datasets before de-batching. (**B**) Gene expression levels statistics of the integrated dataset after de-batching. (**C**) Principal component analysis (PCA) between datasets before de-batching. (**D**) PCA of the integrated datasets after de-batching.

https://doi.org/10.2147/IJGM.S530953

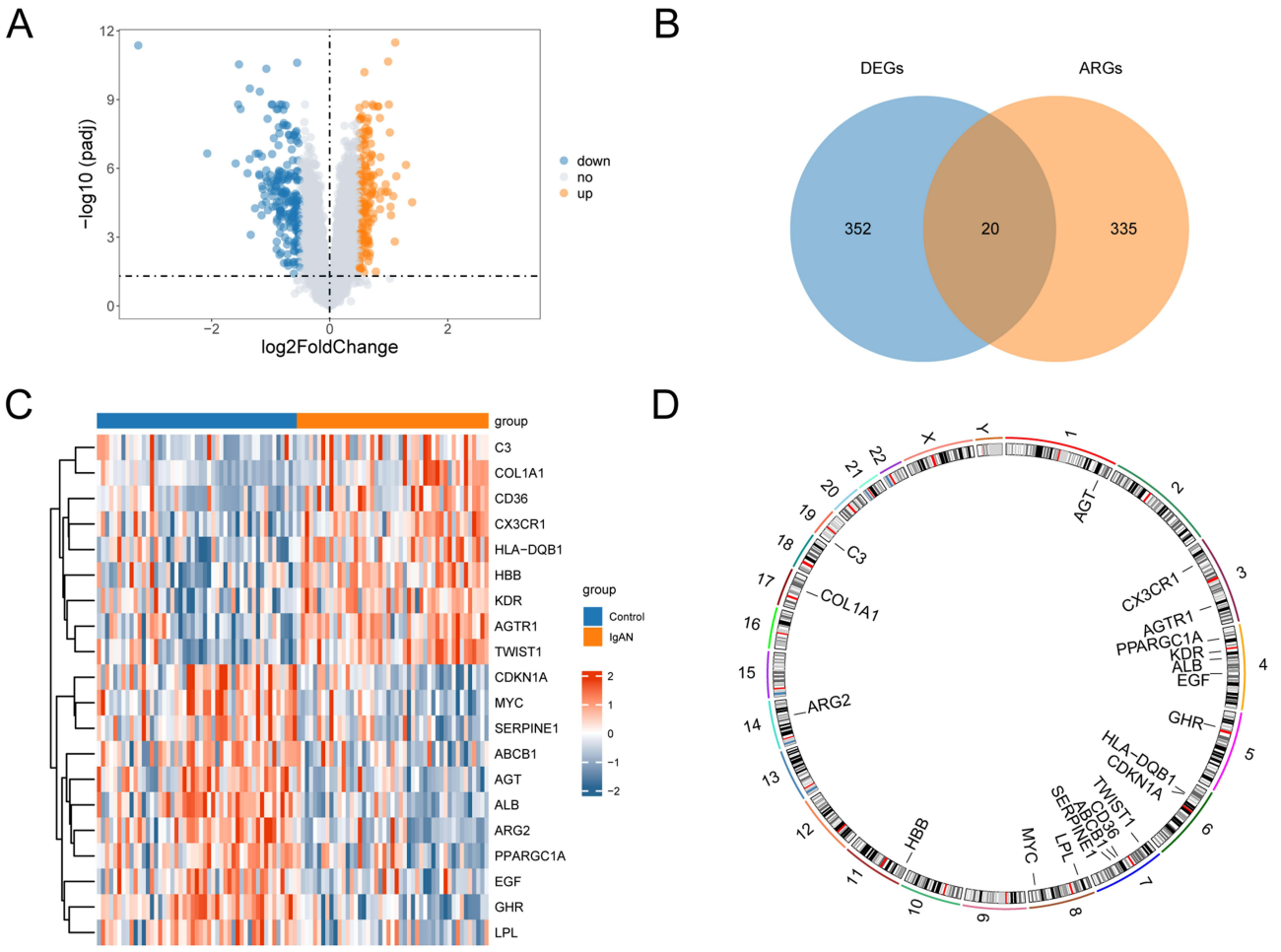

Figure 2 Identification of Aging-related genes (ARGs) and differentially expressed aging-related genes (AR-DEGs). (**A**) Volcano plot of differentially expressed genes (DEGs) between IgAN group and control group in the integrated GEO Datasets. The Orange nodes represent upregulated genes, the blue nodes represent downregulated genes and the gray nodes represent nonsignificant genes; (**B**) Venn diagram of ARGs and DEGs. Blue represents DEGs, orange represents ARGs; (**C**) Heat map of AR-DEGs in the integrated GEO Datasets: orange indicates IgA nephropathy samples, blue indicates normal control samples, red represents high gene expression, and blue represents low gene expression; (**D**) Chromosomal mapping of AR-DEGs.

protein-lipid complex binding. Additionally, GO cellular component (CC) analysis revealed that these genes were mainly focused on platelet alpha granule, blood microparticle, platelet alpha granule lumen, external side of plasma membrane, secretory granule lumen. Furthermore, KEGG pathway analyses exhibited that AR-DEGs were mostly enriched in AGE-RAGE signaling pathway in diabetic complications, proteoglycans in cancer, bladder cancer, PI3K-Akt signaling pathway, endometrial cancer. Figure 4A was the GO/KEGG visual histogram. Meanwhile, the network diagram of BP, CC, MF and KEGG was drawn according to GO and KEGG analysis (Figure 4B–E).

Construction of PPI Network and Identification of Hub Genes

To investigate the interaction relationship among these AR-DEGs, a PPI network was constructed and analyzed using STRING database (Figure 5A). The network showed that there were links between 15 genes, namely: AGT, AGTR1, ALB, C3, CD36, CDKN1A, COL1A1, EGF, GHR, KDR, LPL, MYC, PPARGC1A, SERPINE1, TWIST1. Figure 5B–F shows PPI networks mapped by the top 10 AR-DEGs of the previously mentioned five algorithms. The intersection of the top 10 genes which ranked by previous mentioned methods was hub genes. The hub genes were AGT, ALB, CD36, EGF, KDR, LPL, MYC, and PPARGC1A, respectively (Figure 5G).

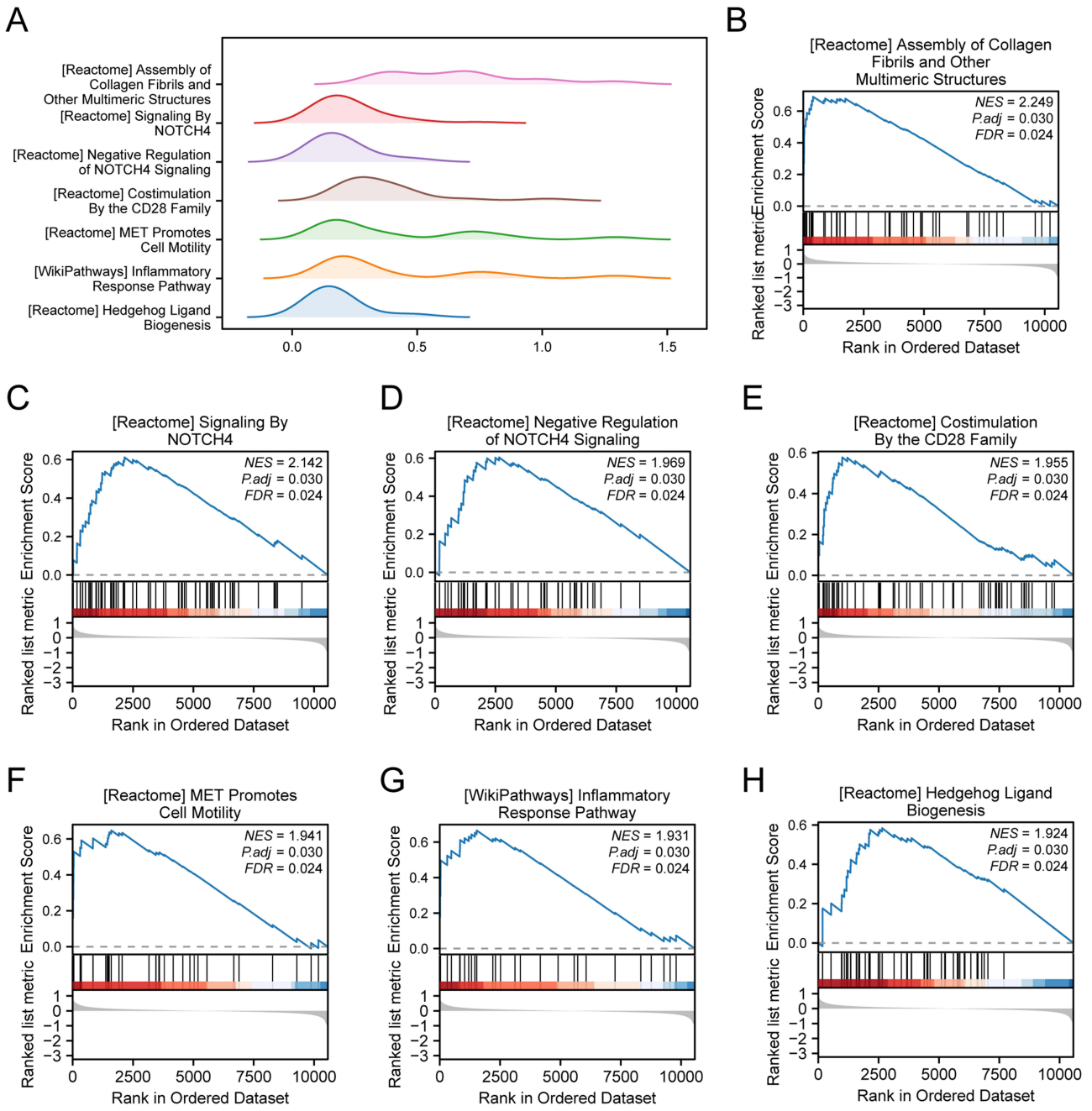

Figure 3 The results of Gene set enrichment analysis (GSEA). (**A**) GSEA method was performed to rank the effects of differentially expressed biological pathways. (**B**) GSEA results of Reactome assembly of collagen fibrils and other multimeric structures chain. (**C**) GSEA results for Reactome signaling by NOTCH4. (**D**) GSEA results of Reactome negative regulation of NOTCH4 signaling chain. (**E**) GSEA results for Reactome costimulation by the CD28 family. (**F**) GSEA results of Reactome MET promotes cell motility chain. (**G**) GSEA results for the wikipathway inflammatory response pathway. (**H**) GSEA results for Reactome hedgehog ligand biogenesis. **Abbreviations**: NES, Normalized Enrichment Score; FDR, False Discovery Rate.

Construction of Regulatory Network

The corresponding TF were obtained by ChIPBase database based on the hub genes, the mRNA-TF regulatory network was constructed and visualized using Cytoscape software, which consisted of 7 nodes and 36 edges (Figure 6A).

Based on these eight AR-DEGs, mRNA-miRNA co-regulatory network was constructed by ENCORI database, and the results showed that the network contained 7 nodes and 51 edges (Figure 6B).

https://doi.org/10.2147/IJGM.S530953

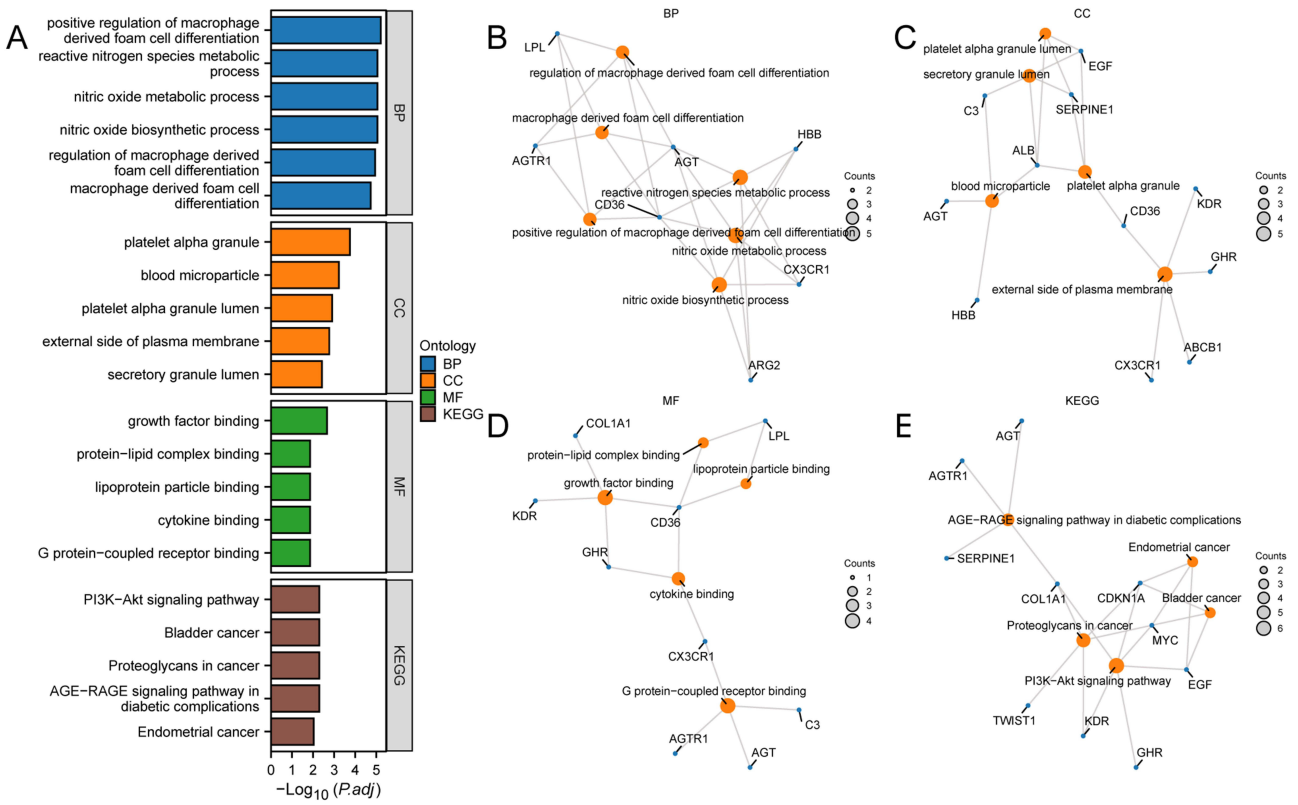

Figure 4 Gene Ontology (GO) and Kyoto Encyclopedia of Genes and Genomes (KEGG) Enrichment Analysis for AR-DEGs. (**A**) Bar graph of GO and KEGG enrichment analysis results of AR-DEGs. (**B**) GO and KEGG enrichment analysis results of AR-DEGs were shown in the network diagram: BP (**B**), CC (**C**), MF (**D**) and KEGG (**E**). The Orange-red nodes represent items, the blue nodes represent molecules, and the lines represent the relationship between items and molecules.
Abbreviations: BP, biological process; CC, cellular component; MF, molecular function.

Expression Level Analysis and ROC Curve Analysis of Hub Genes

Compared with the control group, the expression levels of CD36 and KDR in IgAN group were significantly up-regulated, while the expression levels of AGT, ALB, EGF, LPL, MYC, PPARGC1A were significantly decreased in IgAN group (p value < 0.001) (Figure 7A).

Based on the above analysis, we drew ROC curves and calculated the AUC to validate the diagnostic value of hub genes in the combined datasets. The AUC for AGT, ALB, CD36, EGF, KDR, LPL, MYC, and PPARGC1A in IgAN group and healthy control group were 0.764, 0.818, 0.737, 0.698, 0.766, 0.724, 0.786, and 0.723, respectively (Figure 7B–I).

Immune Infiltration Analysis (CIBERSORT)

The relative abundance of 22 immune cells in IgAN was estimated by the CIBERSORT algorithm. As shown in Figure 8A, the proportion of 22 immune cells was plotted as a histogram. The expression levels of five kinds of immune cells were statistically increased in IgAN group compared with control group, namely macrophages M1, macrophages M2, monocytes, NK cells activated, T cells CD8, whereas B cells naive, neutrophils, NK cells resting, T cells CD4 memory resting were decreased in IgAN group (Figure 8B). The heat map presented the correlation of immune cell infiltration (Figure 8C). The results showed the positive correlation between neutrophils cells and NK cells resting cells (r value = 0.29). T cells CD8 showed an inverse correlation with T cells CD4 memory resting (r value = −0.53). Furthermore, the bubble chart presented in Figure 8D showed that CD36 was positively correlated with monocytes cells but negatively correlated with T cells CD4 memory resting cells (p value < 0.05).

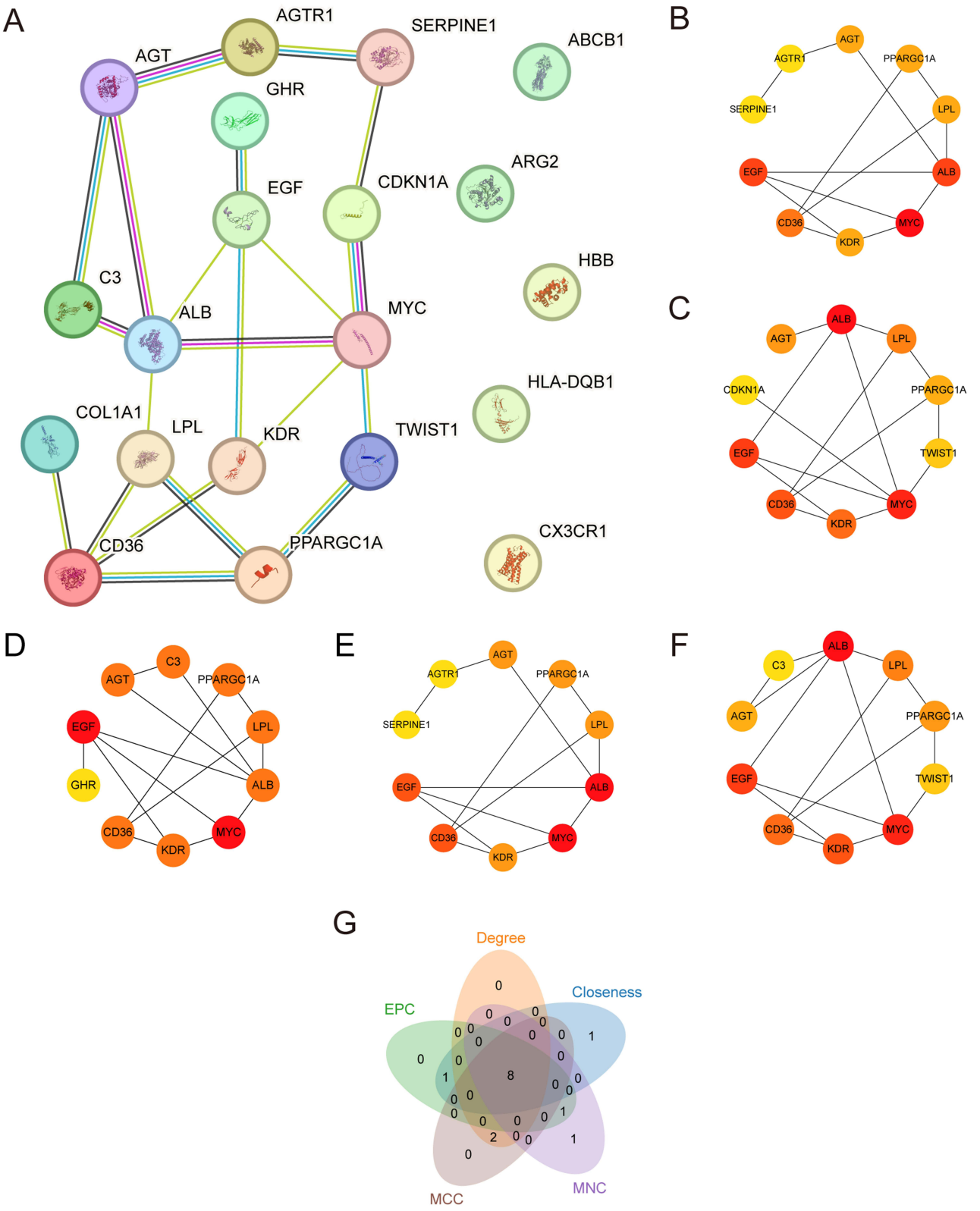

Figure 5 PPI Network and hub genes analysis. (**A**) The PPI Network of AR-DEGs calculated from STRING database. The PPI Network of the top 10 AR-DEGs calculated by the 5 algorithms of the CytoHubba plugin, including MCC (**B**), Closeness (**C**), MNC (**D**), Degree (**E**) and EPC (**F**). (**G**) The Venn diagram of top 10 AR-DEGs by the 5 algorithms of the CytoHubba plugin.

https://doi.org/10.2147/IJGM.S530953

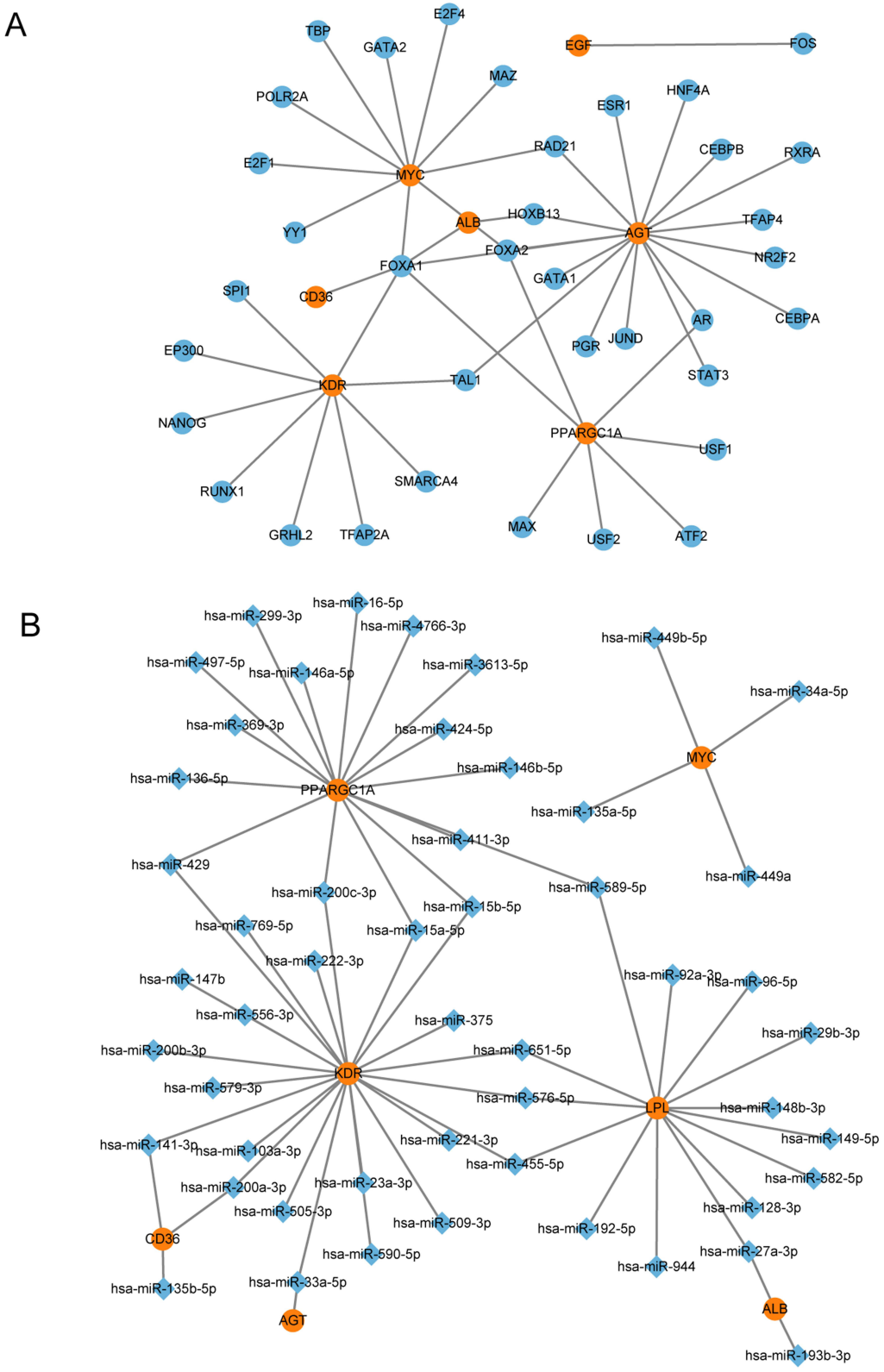

Figure 6 Regulatory Network of hub genes. (**A**) Network for TF-gene interaction with hub genes. (**B**) Gene-miRNA co-regulation network. The orange color nodes indicate hub genes, the blue nodes indicate TF, and the blue diamonds for miRNA.
Abbreviation: TF, Transcription Factor.

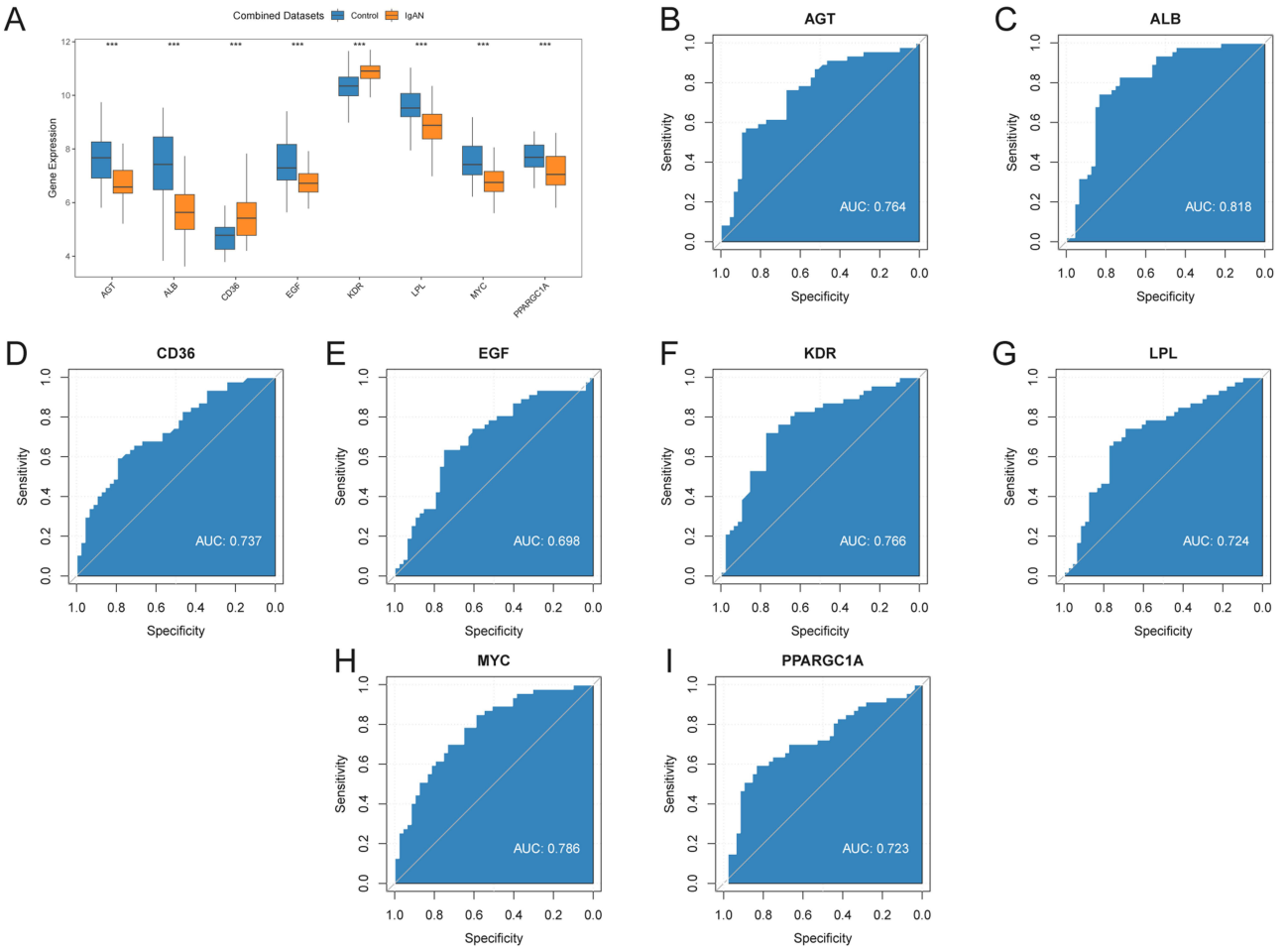

Figure 7 Differential Expression Validation and ROC Curve Analysis. (**A**) the expression levels of hub genes between IgAN and control. ROC curves of AGT (**B**), ALB (**C**), CD36 (**D**), EGF (**E**), KDR (**F**), LPL (**G**), MYC (**H**) and PPARGC1A (**I**) in IgAN. ***represents p value < 0.001.
Abbreviation: ROC, Receiver Operating Characteristic Curve.

mRNA Expression of Hub Genes in IgAN Patients Using Nephroseq V5 Online Platform

The results showed that the expression levels of five hub genes (AGT, ALB, EGF, LPL, PPARGC1A) were significantly decreased in the glomerular tissues of IgAN patients, while that of CD36 and KDR were significantly increased compared with healthy living donors. In addition, comparing with the control group, the expression levels of MYC were significantly downregulated in the renal tubular tissues of IgAN patients (Figure 9).

The Validation of CD36 in IgAN

The above results revealed that CD36 had a relatively higher expression and the higher diagnostic value as well as the close correlation with immune infiltration. Based on this, CD36 was further verified in the kidney tissues of IgAN patients. The results showed that CD36 was highly expressed in the kidney tissues of IgA nephropathy patients compared to the control group (Figure 10).

https://doi.org/10.2147/IJGM.S530953

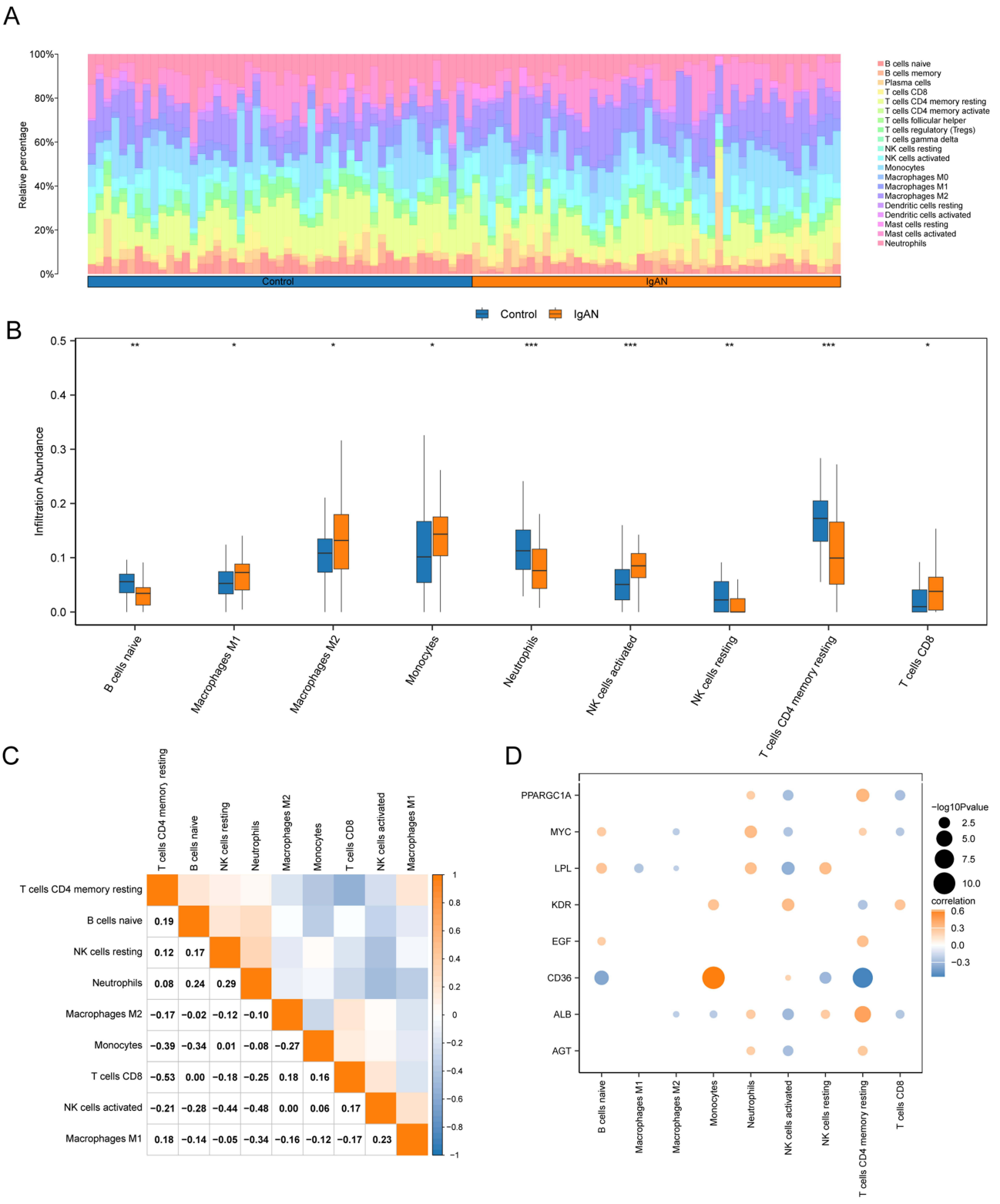

Figure 8 Immune infiltration analysis by CIBERSORT Algorithm in IgAN and control group. The proportion of immune cells in each sample was showed in a histogram (**A**) and group comparison graph (**B**). (**C**) The correlation of 22 types of immune cells in IgAN renal tissues was evaluated. Red: positive correlation, blue: negative correlation. (**D**) Bubble plot of correlation between hub genes and immune cell in IgAN. ns stands for p value ≥ 0.05, not statistically significant; *represents p value < 0.05; **represents p value < 0.01; ***represents p value < 0.001.

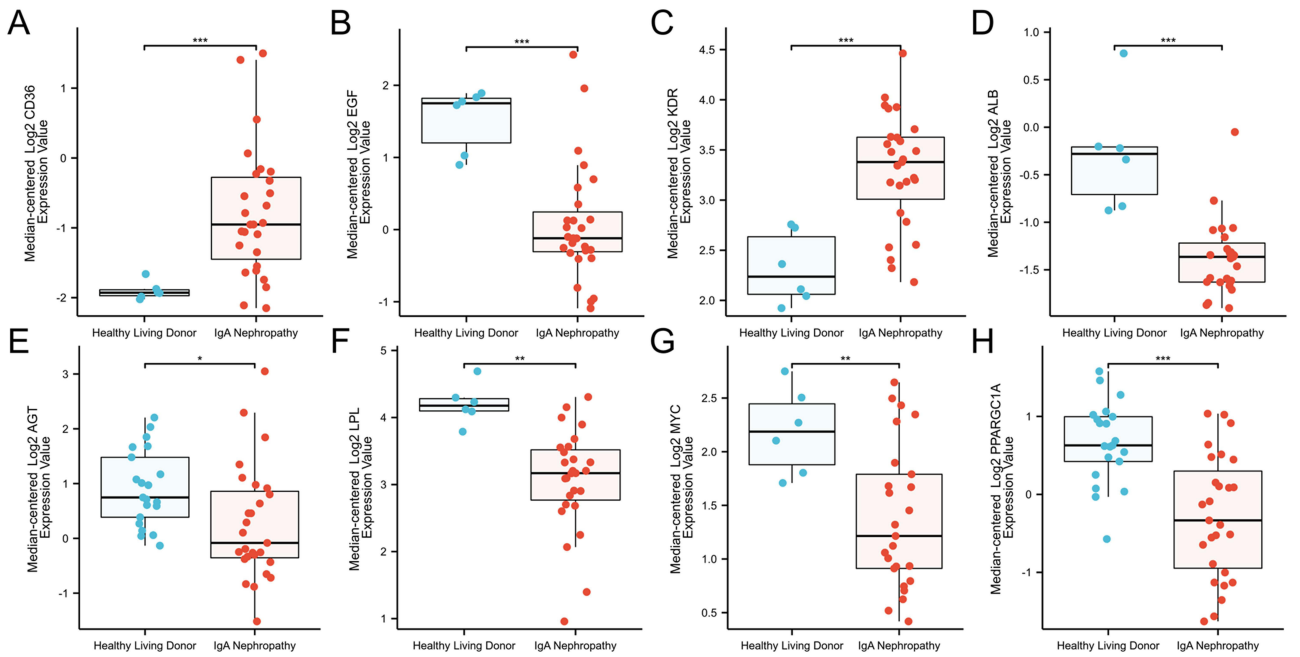

Figure 9 Differential expression of hub genes between IgAN group and normal group in the Nephroseq v5 database. (**A**) The expression of CD36 in IgAN group was higher than that of normal control. (**B**) The expression of EGF in IgAN group was reduced than that of normal control. (**C**) The expression of KDR in IgAN group was higher than that of normal control. (**D**) The expression of ALB in IgAN group was reduced than that of normal control. (**E**) The expression of AGT in IgAN group was reduced than that of normal control. (**F**) The expression of LPL in IgAN group was reduced than that of normal control. (**G**) The expression of MYC in IgAN group was reduced than that of normal control. (**H**) The expression of PPARGC1A in IgAN group was reduced than that of normal control. $p < 0.05$ was considered statistically significant. *$p < 0.05$; **$p < 0.01$; ***$p < 0.001$.

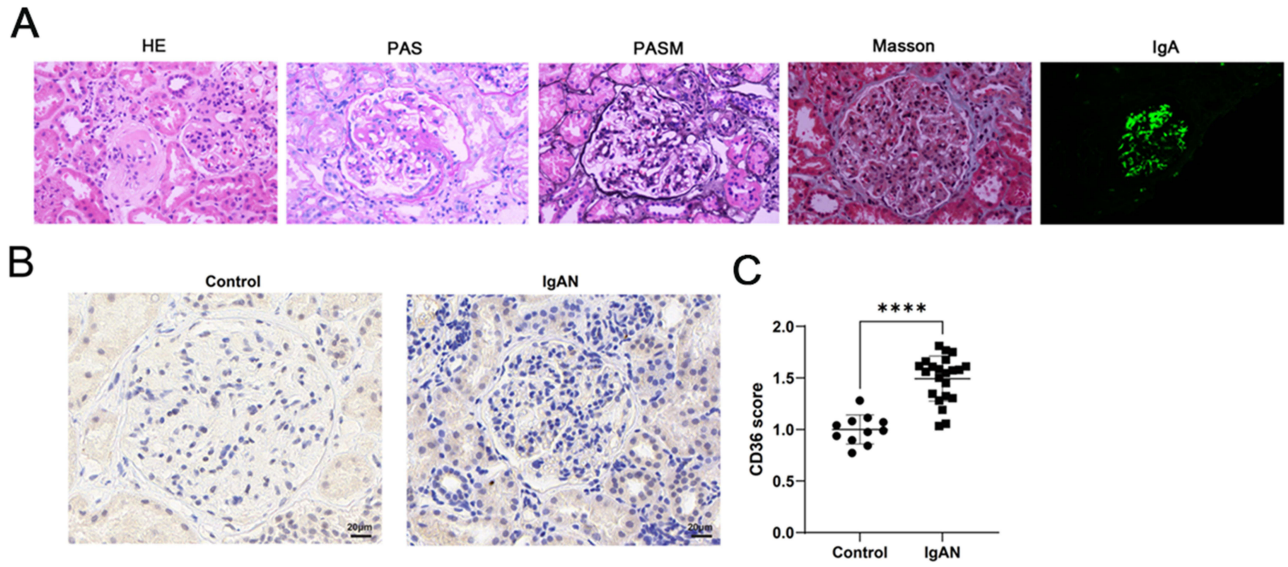

Figure 10 Validation of Pathological and CD36 in IgAN (IgA nephropathy) patients. (**A**) Histopathological diagnosis of clinical IgA nephropathy demonstrated by renal tissue structural and immunological changes visualized through hematoxylin and eosin (HE, original magnification×400), periodic acid-Schiff (PAS, original magnification×400), periodic acid-Schiff methenamine (PASM, original magnification×400), and Masson's trichrome (MASSON,×400) staining techniques. (**B**) Immunohistochemistry validation of CD36 expression in IgAN patients and controls. (**C**) Quantitative analysis showing a significant increase in CD36 expression in IgAN patients compared with controls. ****$p < 0.0001$.

https://doi.org/10.2147/IJGM.S530953

Discussion

The phenotypic manifestation of IgAN is highly variable, ranging from asymptomatic microscopic hematuria to rapidly progressive glomerulonephritis. The heterogeneity of clinical presentation and outcome makes it challenging to predict disease progression and treatment response. Lu et al reported that human IgAN was associated with increased telomere shortening and related inflammatory proteins secretion.[29] These findings suggested that telomere shortening was associated with the progression of IgAN. Given that shortening of telomere length was considered one of the indicators of aging, these findings suggested that aging was a risk factor for IgAN,[30,31] the exact pathophysiological mechanism of aging exacerbating IgAN remains unclear. It is important to actively understand the underlying mechanisms of aging-related IgAN to develop new therapeutic strategies. Therefore, the primary purpose of the present study was to identify potential aging biomarkers in IgAN and to explore the underlying mechanism and role of aging-related genes and immune infiltration in IgAN, so as to provide new strategy and supporting evidence for the potential mechanisms and early diagnosis of IgAN.

In this study, hub genes were selected through the construction of PPI network and the selection of five algorithms: MCC, Closeness, MNC, Degree and EPC. The genes were AGT, ALB, CD36, EGF, KDR, LPL, MYC, PPARGC1A, respectively. Furthermore, compared with the normal control group, the expression levels of CD36 and KDR were higher in IgAN patients, while the expression levels of AGT, ALB, LPL, MYC and PPARGC1A were lower. Nephroseq database also verified the differences in expression of these genes between normal population and IgAN patients. The increased expression of CD36 was further verified on the kidney tissues of patients with IgAN by immunohistochemistry. In particular, immune cell infiltration analysis showed that CD36 was significantly correlated with multiple immune cells. This suggested that the expression of these genes was closely related to the progression of IgAN, especially CD36 may be a potential new therapeutic target for IgAN.

CD36 is a transmembrane glycoprotein that belongs to a family of class B scavenger receptors. Recently, a growing number of studies had shown that CD36 binds a variety of ligands, and thus participates in a diverse range of pathophysiological processes, such as lipid metabolism, inflammation, atherosclerosis. With the advancement of research, CD36 played an important role in a number of kidney disease. Firstly, CD36 overexpression led to lipid accumulation by increasing fatty acid uptake in renal tubular epithelial cells of chronic kidney disease(CKD) model mice and podocytes cultured in vitro.[32–34] Importantly, fatty acid accumulation and alterations in the lipid metabolism may result in glomerular and tubular cell injury.[35] In hypoxic dendritic cells, blocking CD36 markedly reduced lipid uptake and accumulation, eliminated NKT cell overactivation, and reversed renal ischemia-reperfusion injury intensification.[36] Secondly, CD36 mediated the endocytosis and degradation of oxidized low-density lipoprotein (ox-LDL) in macrophages. Ox-LDL deposition was up-regulated in the renal tubules and interstitial compartment and correlated with fibrosis in hypercholesterolaemic mice with kidney injury following unilateral ureteral obstruction (UUO).[37] Additionally, knockout of CD36 gene significantly decreased oxidative stress and inflammatory pathway, thus ameliorating renal fibrosis. Compared with wild-type mice, CD36-deficient mice not only demonstrated reduced levels of activated NF-κB and oxidative stress, but also decreased interstitial myofibroblasts accumulation in a hypercholesterolemic model of CKD.[33,38] In addition, CD36 has been demonstrated to be involved in the endocytosis of many substance such as advanced oxidation protein products (AOPP), Advanced glycation end-products (AGEs). Previous studies indicated that binding of AOPP to CD36 induced renal RAS activation via the PKCα-NADPH oxidase-AP-1 /NF-κB pathway. When CD36 was blocked, the results showed that AOPP-induced NADPH oxidase activation and ROS production were significantly inhibited.[39] Anti-CD36 antibody treatment significantly inhibited the endocytic association and degradation of AOPPs-HSA in vitro in cultured HK-2 cells. In addition to this, AOPPs endocytosis increased the production of reactive oxygen species and the secretion of transforming growth factor (TGF)-β1 in HK-2 cells, whereas the upregulation of TGF-β1 was neutralized in the presence of anti-CD36 antibodies.[40] Based on the above results, it was suggested that CD36 mediated the renal damage effect of AOPPs. AGEs accumulate had been observed during aging and age-related diseases.[41] Some studies had showed that AGEs enhance the foam cell formation and CD36 expression in macrophages through oxidative stress generation.[42,43] AGE-RAGE-induced oxidative stress generation stimulated ox-LDL uptake into macrophages via the Cdk5-CD36 pathway. These findings showed that CD36 play

a significant role in the endocytosis of AGEs. Besides that, the expression of CD36 and NLRP3 were reported to be up-regulated in the podocytes of patients with lupus nephritis. Knocking out CD36 in podocytes reduced the levels of NLRP3 inflammasome, increased the autophagy levels and alleviated podocyte injury, the present findings supported a link between autophagy and CD36.[44] In our study, the result showed that the expression of CD36 was increased in the kidney tissues of IgAN compared to the control group. Consistent with this, recently, it has been reported that CD36 was involved in the regulation of autophagy in IgAN.[45] Studies had shown that CD36 expression was positively correlated with 24-hour proteinuria, serum creatinine, renal fibrosis-related and autophagy-related factors in IgAN. After pIgA1 stimulation, CD36 and fibrosis-related factors in mouse mesangial cells were significantly increased. When CD36 was knocked down, the pIgA1-stimulated mouse mesangial cells extracellular matrix accumulation was reduced. Previous studies on the mechanism of CD36 in kidney disease were mostly seen in CKD and diabetic kidney disease. We speculate that CD36 aggravate renal lipid deposition and mediate renal cell lipid peroxidation by increasing oxidative stress and activating inflammatory response, which may contribute to the aggravation of glomerular sclerosis, podocyte injury, and promote renal fibrosis, thereby aggravating IgA nephropathy. More research is needed to further elucidate the specific molecular mechanisms in the future.

In agreement with previous findings, our result showed that AGT gene was down-regulated in IgAN by integrated bioinformatics analysis.[46,47] ALB was reported that every 1g/L decrease in time-mean serum albumin (TA-ALB) levels, the risk of renal progression increased by 14%.[48] Consistent with the previous findings,[49] we found that ALB was down-regulated in IgAN. In our study, our finding that IgAN patients had lower EGF levels than healthy individuals was consistent with previously reported results.[50] Our results were consistent with previous studies in which MYC expression was down-regulated in IgAN.[47,51] In addition, it has been reported that in familial IgAN, MYC was a key gene modulator of the WNT/β-catenin and PI3K/AKT pathways, which were also one of the pathogenesis of IgAN.[52] Our result showed that the expressions of KDR, LPL and PPARGC1A were decreased in IgAN patients compared to normal group. However, no relevant studies have been reported in IgAN at present, and further studies are needed in the future.

There is growing evidence suggesting the crucial role of immune system in the pathogenesis of IgAN. Our immune infiltration analysis revealed significant differences in 9 types of immune cells between IgAN patients and control, suggesting a specific immune landscape associated with the disease. Our results indicated a increased infiltration of macrophages M1, macrophages M2, monocytes, NK cells activated, T cells CD8, along with an decreased infiltration of B cells naive, T cells CD4 memory resting, NK cells resting, neutrophils, suggesting that these immune cells may be involved in the pathogenesis of IgAN. It is worth noting that the number and subtypes of macrophages were correlated with the clinical manifestations and pathology of IgAN patients, and they may contribute to renal sclerosis, glomerular injury and renal fibrosis through the production of pro-inflammatory cytokines, growth and fibrotic factors.[53,54] T cells were another pivotal component of the adaptive immune response in IgAN. Many studies have confirmed that most T cell subpopulations were associated with the clinical features of IgAN.[55,56] Their involvement was also noteworthy given the role of B cells in IgA production and immune complex formation, both of which were central features of IgAN pathogenesis. In addition, studies have confirmed that immunomodulators targeting B cells can significantly improve IgAN, regulate the secretion of cytokines and chemokines, and delay the progression of the disease.[57,58] CD36 was associated with multiple immune cell subpopulations in kidney tissue of IgAN patients, suggesting that CD36 not only serve as a potential biomarker for diagnosis, but also offer a window into understanding how genetic regulation intersects with immune processes to drive disease progression.

Despite the promising findings of our research, there are several limitations that may impact the interpretation and applicability of our results. Firstly, this study was based on the previously published data set for secondary utilization and analysis. Secondly, due to the small sample size of clinical patients, we did not perform the correlation analysis between CD36 and age. Thirdly, a key limitation of our study was the reliance on specific GEO datasets and the Nephroseq database for initial validation. To strengthen the clinical relevance and generalizability of our findings, future validation in larger, independent, and prospectively collected IgAN patient cohorts, encompassing diverse demographics and disease severities, is essential. Further experimental and clinical studies are required to validate the results and clarify the molecular mechanisms underlying the observed associations.

Conclusions

In conclusion, 20 AR-DEGs were identified in IgAN from the perspective of bioinformatics analysis, which were mainly enriched in regulation of macrophage derived foam cell differentiation, AGE-RAGE signaling pathway in diabetic complications, PI3K-Akt signaling pathway. Our study also suggested a correlation between the expression levels of these genes and the proportion of infiltrating immune cells in patients with IgAN. CD36 demonstrated diagnostic value in IgAN and represented a potential biomarker for this disease.

Data Sharing Statement

Summary statistics can be downloaded from the appropriate website (see Materials and methods for details). Further inquiries and requests can be directed to the corresponding author.

Ethical Statement and Consent

The studies concerning human participants were approved by Medical Ethics Committee of the Second People's Hospital of Hefei (2024-062). Participants provided written informed consent prior to study enrolment. All experiments were performed in accordance with the Declaration of Helsinki.

Acknowledgments

We acknowledge GEO database for providing their platforms and contributors for uploading their meaningful datasets. We are very grateful to all the participants in this study. This paper has been uploaded to Medrxiv as a preprint: (https://www.medrxiv.org/content/10.1101/2025.02.20.25322599v1).

Funding

This work was supported by the hospital-level fund of the Second People's Hospital of Hefei (2024ykc013).

Disclosure

The authors report no competing interests to declare for this work.

References

1. Wyatt RJ, Julian BA. IgA nephropathy. *N Engl J Med*. 2013;368(25):2402–2414. doi:10.1056/NEJMra1206793
2. Xie J, Chen N. Primary glomerulonephritis in mainland China: an overview. *Contrib Nephrol*. 2013;181:1–11. doi:10.1159/000348642
3. Radford MG Jr, Donadio JV Jr, Bergstralh EJ, Grande JP. Predicting renal outcome in IgA nephropathy. *J Am Soc Nephrol*. 1997;8(2):199–207. doi:10.1681/ASN.V82199
4. Goto M, Wakai K, Kawamura T, Ando M, Endoh M, Tomino Y. A scoring system to predict renal outcome in IgA nephropathy: a nationwide 10-year prospective cohort study. *Nephrol Dial Transplant*. 2009;24(10):3068–3074. doi:10.1093/ndt/gfp273
5. Berthoux FC, Mohey H, Afiani A. Natural history of primary IgA nephropathy. *Semin Nephrol*. 2008;28(1):4–9. doi:10.1016/j.semnephrol.2007.10.001
6. Wang K, Liu H, Hu Q, et al. Epigenetic regulation of aging: implications for interventions of aging and diseases. *Signal Transduct Target Ther*. 2022;7(1):374. doi:10.1038/s41392-022-01211-8
7. Rossiello F, Jurk D, Passos JF, d'Adda Di Fagagna F. Telomere dysfunction in ageing and age-related diseases. *Nat Cell Biol*. 2022;24(2):135–147. doi:10.1038/s41556-022-00842-x
8. Stevens LA, Viswanathan G, Weiner DE. Chronic kidney disease and end-stage renal disease in the elderly population: current prevalence, future projections, and clinical significance. *Adv Chronic Kidney Dis*. 2010;17(4):293–301. doi:10.1053/j.ackd.2010.03.010
9. Fofi C, Pecci G, Galliani M, et al. IgA nephropathy: multivariate statistical analysis aimed at predicting outcome. *J Nephrol*. 2001;14(4):280–285.
10. Duan ZY, Cai GY, Chen YZ, et al. Aging promotes progression of IgA nephropathy: a systematic review and meta-analysis. *Am J Nephrol*. 2013;38(3):241–252. doi:10.1159/000354646
11. Oshima Y, Moriyama T, Itabashi M, Takei T, Nitta K. Characteristics of IgA nephropathy in advanced-age patients. *Int Urol Nephrol*. 2015;47(1):137–145. doi:10.1007/s11255-014-0872-1
12. Cheungpasitporn W, Nasr SH, Thongprayoon C, Mao MA, Qian Q. Primary IgA nephropathy in elderly patients. *Nephrology*. 2015;20(6):419–425. doi:10.1111/nep.12440
13. Wen YK, Chen ML. Differences in new-onset IgA nephropathy between young adults and the elderly. *Ren Fail*. 2010;32(3):343–348. doi:10.3109/08860221003611687
14. Okabayashi Y, Tsuboi N, Haruhara K, et al. Reduction of proteinuria by therapeutic intervention improves the renal outcome of elderly patients with IgA nephropathy. *Clin Exp Nephrol*. 2016;20(6):910–917. doi:10.1007/s10157-016-1239-y

15. Spanish Group for the Study of Glomerular Diseases (GLOSEN); Sevillano AM, Diaz M, Caravaca-Fontán F, et al. IgA nephropathy in elderly patients. *Clin J Am Soc Nephrol*. 2019;14(8):1183–1192. doi:10.2215/CJN.13251118
16. Gentile M, Sanchez-Russo L, Riella LV, et al. Immune abnormalities in IgA nephropathy. *Clin Kidney J*. 2023;16(7):1059–1070. doi:10.1093/ckj/sfad025
17. Du W, Gao CY, You X, et al. Increased proportion of follicular helper T cells is associated with B cell activation and disease severity in IgA nephropathy. *Front Immunol*. 2022;13:901465. doi:10.3389/fimmu.2022.901465
18. Borgoni S, Kudryashova KS, Burka K, de Magalhães JP. Targeting immune dysfunction in aging. *Ageing Res Rev*. 2021;70:101410. doi:10.1016/j.arr.2021.101410
19. Stelzer G, Rosen N, Plaschkes I, et al. The genecards suite: from gene data mining to disease genome sequence analyses. *Curr Protoc Bioinformatics*. 2016;54:1.30.1–1.30.33. doi:10.1002/cpbi.5
20. Liberzon A, Subramanian A, Pinchback R, Thorvaldsdóttir H, Tamayo P, Mesirov JP. Molecular signatures database (MSigDB) 3.0. *Bioinformatics*. 2011;27(12):1739–1740. doi:10.1093/bioinformatics/btr260
21. Berthier CC, Bethunaickan R, Gonzalez-Rivera T, et al. Cross-species transcriptional network analysis defines shared inflammatory responses in murine and human lupus nephritis. *J Immunol*. 2012;189(2):988–1001. doi:10.4049/jimmunol.1103031
22. Liu P, Lassén E, Nair V, et al. Transcriptomic and proteomic profiling provides insight into mesangial cell function in IgA nephropathy. *J Am Soc Nephrol*. 2017;28(10):2961–2972. doi:10.1681/ASN.2016101103
23. Subramanian A, Tamayo P, Mootha VK, et al. Gene set enrichment analysis: a knowledge-based approach for interpreting genome-wide expression profiles. *Proc Natl Acad Sci U S A*. 2005;102(43):15545–15550. doi:10.1073/pnas.0506580102
24. Szklarczyk D, Gable AL, Lyon D, et al. STRING v11: protein-protein association networks with increased coverage, supporting functional discovery in genome-wide experimental datasets. *Nucleic Acids Res*. 2019;47(D1):D607–D613. doi:10.1093/nar/gky1131
25. Zhou KR, Liu S, Sun WJ, et al. ChIPBase v2.0: decoding transcriptional regulatory networks of non-coding RNAs and protein-coding genes from ChIP-seq data. *Nucleic Acids Res*. 2017;45(D1):D43–D50. doi:10.1093/nar/gkw965
26. Li JH, Liu S, Zhou H, Qu LH, Yang JH. starBase v2.0: decoding miRNA-ceRNA, miRNA-ncRNA and protein-RNA interaction networks from large-scale CLIP-Seq data. *Nucleic Acids Res*. 2014;42(Database issue):D92–7. doi:10.1093/nar/gkt1248
27. Newman AM, Liu CL, Green MR, et al. Robust enumeration of cell subsets from tissue expression profiles. *Nat Methods*. 2015;12(5):453–457. doi:10.1038/nmeth.3337
28. Eddy S, Mariani LH, Kretzler M. Integrated multi-omics approaches to improve classification of chronic kidney disease. *Nat Rev Nephrol*. 2020;16(11):657–668. doi:10.1038/s41581-020-0286-5
29. Lu YY, Yang X, Chen WQ, et al. Proteins induced by telomere dysfunction are associated with human IgA nephropathy. *J Zhejiang Univ Sci B*. 2014;15(6):566–574. doi:10.1631/jzus.B1300115
30. Zhang Y, Li Q, Shi S, et al. Clinical and pathological characteristics in elderly patients with IgA nephropathy. *Clin Kidney J*. 2023;16(11):1974–1979. doi:10.1093/ckj/sfad203
31. Wen Q, Rong R, Zhou Q, et al. Clinical, pathological characteristics and outcomes of immunoglobulin A nephropathy patients with different ages. *Nephrology*. 2020;25(12):906–912. doi:10.1111/nep.13667
32. Hua W, Huang HZ, Tan LT, et al. CD36 mediated fatty acid-induced podocyte apoptosis via oxidative stress. *PLoS One*. 2015;10(5):e0127507. doi:10.1371/journal.pone.0127507
33. Okamura DM, Pennathur S, Pasichnyk K, et al. CD36 regulates oxidative stress and inflammation in hypercholesterolemic CKD. *J Am Soc Nephrol*. 2009;20(3):495–505. doi:10.1681/ASN.2008010009
34. Hua W, Peng L, Chen XM, et al. CD36-mediated podocyte lipotoxicity promotes foot process effacement. *Open Med*. 2024;19(1):20240918. doi:10.1515/med-2024-0918
35. Mitrofanova A, Merscher S, Fornoni A. Kidney lipid dysmetabolism and lipid droplet accumulation in chronic kidney disease. *Nat Rev Nephrol*. 2023;19(10):629–645. doi:10.1038/s41581-023-00741-w
36. Qu J, Li D, Jin J, et al. Hypoxia-inducible factor 2α attenuates renal ischemia-reperfusion injury by suppressing CD36-mediated lipid accumulation in dendritic cells in a mouse model. *J Am Soc Nephrol*. 2023;34(1):73–87. doi:10.1681/ASN.0000000000000027
37. Okamura DM, López-Guisa JM, Koelsch K, Collins S, Eddy AA. Atherogenic scavenger receptor modulation in the tubulointerstitium in response to chronic renal injury. *Am J Physiol Renal Physiol*. 2007;293(2):F575–85. doi:10.1152/ajprenal.00063.2007
38. Pennathur S, Pasichnyk K, Bahrami NM, et al. The macrophage phagocytic receptor CD36 promotes fibrogenic pathways on removal of apoptotic cells during chronic kidney injury. *Am J Pathol*. 2015;185(8):2232–2245. doi:10.1016/j.ajpath.2015.04.016
39. Cao W, Xu J, Zhou ZM, Wang GB, Hou FF, Nie J. Advanced oxidation protein products activate intrarenal renin-angiotensin system via a CD36-mediated, redox-dependent pathway. *Antioxid Redox Signal*. 2013;18(1):19–35. doi:10.1089/ars.2012.4603
40. Iwao Y, Nakajou K, Nagai R, et al. CD36 is one of important receptors promoting renal tubular injury by advanced oxidation protein products. *Am J Physiol Renal Physiol*. 2008;295(6):F1871–80. doi:10.1152/ajprenal.00013.2008
41. Zgutka K, Tkacz M, Tomasiak P, Tarnowski M. A role for advanced glycation end products in molecular ageing. *Int J Mol Sci*. 2023;24(12):9881. doi:10.3390/ijms24129881
42. Terasaki M, Yashima H, Mori Y, et al. A dipeptidyl peptidase-4 inhibitor inhibits foam cell formation of macrophages in type 1 diabetes via suppression of CD36 and ACAT-1 expression. *Int J Mol Sci*. 2020;21(13):4811. doi:10.3390/ijms21134811
43. Yashima H, Terasaki M, Sotokawauchi A, et al. AGE-RAGE axis stimulates oxidized LDL uptake into macrophages through cyclin-dependent kinase 5-CD36 pathway via oxidative stress generation. *Int J Mol Sci*. 2020;21(23):9263. doi:10.3390/ijms21239263
44. Lv F, He Y, Xu H, et al. CD36 aggravates podocyte injury by activating NLRP3 inflammasome and inhibiting autophagy in lupus nephritis. *Cell Death Dis*. 2022;13(8):729. doi:10.1038/s41419-022-05179-9
45. Zhang J, Wang Y, Chen C, Liu X, Liu X, Wu Y. Downregulation of CD36 alleviates IgA nephropathy by promoting autophagy and inhibiting extracellular matrix accumulation in mesangial cells. *Int Immunopharmacol*. 2025;144:113672. doi:10.1016/j.intimp.2024.113672
46. Chen X, Sun M. Identification of key genes, pathways and potential therapeutic agents for IgA nephropathy using an integrated bioinformatics analysis. *J Renin Angiotensin Aldosterone Syst*. 2020;21(2):1470320320919635. doi:10.1177/1470320320919635

47. Noor F, Saleem MH, Aslam MF, Ahmad A, Aslam S. Construction of miRNA-mRNA network for the identification of key biological markers and their associated pathways in IgA nephropathy by employing the integrated bioinformatics analysis. *Saudi J Biol Sci*. 2021;28(9):4938–4945. doi:10.1016/j.sjbs.2021.06.079
48. Ni Z, Yuan Y, Wang Q, et al. Time-averaged albumin predicts the long-term prognosis of IgA nephropathy patients who achieved remission. *J Transl Med*. 2014;12:194. doi:10.1186/1479-5876-12-194
49. Li X, Zeng M, Liu J, et al. Identifying potential biomarkers for the diagnosis and treatment of IgA nephropathy based on bioinformatics analysis. *BMC Med Genomics*. 2023;16(1):63. doi:10.1186/s12920-023-01494-y
50. Wang X, Bove AM, Simone G, Ma B. Molecular bases of VEGFR-2-mediated physiological function and pathological role. *Front Cell Dev Biol*. 2020;8:599281. doi:10.3389/fcell.2020.599281
51. Zhang H, Lu H, Zhan B, Shi H, Shui B. Comprehensive analysis of ceRNA network and immune cell infiltration pattern of autophagy-related genes in IgA nephropathy. *Kidney Blood Press Res*. 2024;49(1):528–547. doi:10.1159/000539571
52. Cox SN, Pesce F, El-Sayed Moustafa JS, et al. European IgAN consortium. Multiple rare genetic variants co-segregating with familial IgA nephropathy all act within a single immune-related network. *J Intern Med*. 2017;281(2):189–205. doi:10.1111/joim.12565
53. Liu Y, Gong Y, Xu G. The role of mononuclear phagocyte system in IgA nephropathy: pathogenesis and prognosis. *Front Immunol*. 2023;14:1192941. doi:10.3389/fimmu.2023.1192941
54. Ding Y, Li H, Xu L, Wang Y, Yang H. Bioinformatics Analyses. *Front Mol Biosci*. 2022;9:884588. doi:10.3389/fmolb.2022.884588
55. Ruszkowski J, Lisowska KA, Pindel M, Heleniak Z, Dębska-ślizień A, Witkowski JM. T cells in IgA nephropathy: role in pathogenesis, clinical significance and potential therapeutic target. *Clin Exp Nephrol*. 2019;23(3):291–303. doi:10.1007/s10157-018-1665-0
56. Xie S, Sun M, Zhang X, et al. T cell responses in immune-mediated IgA nephropathy. *J Leukoc Biol*. 2024;116(3):523–535. doi:10.1093/jleuko/qiae103
57. NefIgArd Trial Investigators, Barratt J, Lafayette R, Kristensen J, et al. Results from part A of the multi-center, double-blind, randomized, placebo-controlled NefIgArd trial, which evaluated targeted-release formulation of budesonide for the treatment of primary immunoglobulin A nephropathy. *Kidney Int*. 2023;103(2):391–402. doi:10.1016/j.kint.2022.09.017
58. Lv J, Liu L, Hao C, et al. Randomized phase 2 trial of telitacicept in patients with IgA nephropathy with persistent proteinuria. *Kidney Int Rep*. 2022;8(3):499–506. doi:10.1016/j.ekir.2022.12.014